

Technical Note

# Knowledge-Based Generalized Side-Lobe Canceller for Ionospheric Clutter Suppression in HFSWR

Xin Zhang <sup>1,2</sup>, Di Yao <sup>1</sup>, Qiang Yang <sup>1,2</sup>, Yingning Dong <sup>1,2</sup> and Weibo Deng <sup>1,2,\*</sup>

<sup>1</sup> School of Electronics Information Engineering, Harbin Institute of Technology, 92# West Dazhi Street, Harbin 150001, China; zhangxinhit@hit.edu.cn (X.Z.); yaodi1988@126.com (D.Y.); yq@hit.edu.cn (Q.Y.); dongyn@hit.edu.cn (Y.D.)

<sup>2</sup> Collaborative Innovation Center of Information Sensing and Understanding at Harbin Institute of Technology, Harbin 150001, China

\* Correspondence: dengweibo@hit.edu.cn; Tel.: +86-451-86418052

Received: 30 October 2017; Accepted: 12 January 2018; Published: 13 January 2018

**Abstract:** High frequency surface wave radar (HFSWR) has been successfully developed for early warning and remote sensing. However, the ionospheric clutter is a difficult challenge that can make HFSWR system inefficient. The Generalized Side-lobe Canceller (GSC) has been proved to be an effective algorithm for clutter suppression in theory, but it suffers from the performance degradation for some non-ideal conditions in practice. The most intolerable shortcoming is the signal to noise ratio (SNR) loss caused by the residual signal in the secondary data. In this paper, a knowledge-based GSC (KB-GSC) method has been proposed via an adaptive single notch filter design to reject the residual signal for reducing the SNR loss. The feasibility and availability has been demonstrated by measured data.

**Keywords:** HFSWR; ionospheric clutter; GSC; knowledge based

## 1. Introduction

High frequency surface wave radar (HFSWR) can provide the capabilities of targets monitoring and ocean remote sensing over the horizon (OTH) by transmitting HF vertical polarization electromagnetic wave working on 3 MHz–30 MHz [1]. However, it works on the congested HF band and faces the complicated electromagnetic environment which includes clutter (such as sea clutter and ionospheric clutter), directional interference (such as radio interference) and the interference from the universe and atmosphere [2].

Ionospheric clutter which is the echo reflected from the ionosphere is the most complex type of clutter for HFSWR [3–5]. It always has strong energy and covers a wide region at a far distance. In this case, it may cause the HFSWR blind for detecting weak targets over the horizon. As such, suppressing the ionospheric clutter for weak target detection over the horizon in HFSWR has drawn much attention.

A large number of effects have been applied to HFSWR [6–8] and a few algorithms or methods have been proposed for ionospheric clutter suppression recently. However, further discussion to meet the real operating environment is still required. The generalized side-lobe canceller (GSC), which is also named as the standard coherent side-lobe cancellation technique (CSLC) [9,10], has been proved to be an effective method in theory, for noise, co-channel communication, and interference in the side-lobe [11–17]. Based on GSC, Wan has made great contribution by constructing a receiving array which consists of a main antenna for receiving echo including signal of interesting (SOI), clutter, interference and noise and several auxiliary antennas for obtaining the information of clutter and interference for clutter suppression in HFSWR [18,19]. However, the proposal of Wan's construction is with only one degree of freedom and it is designed for ocean remote sensing, not for the target

detection. Thus, there is a limitation for target detection due to the limited degree of freedom, as there is only one main antenna, especially in the dense target scene.

In this paper, we focus on the target detection, which are submerged in Es-layer ionospheric clutter which often comes out when the radar working frequency is in the 3–5MHz range [20]. There are two challenges to battle: one is that the freedom of array should be increased for dense targets scene; the other is that several practical conditions in the practical HFSWR system should be concerned carefully. Aiming at these two challenges, this paper is composed as follows: firstly, the framework of the GSC method is introduced in Section 2, including the GSC method and GSC based on the virtual sliding subarray method for greater freedom of the array. The practical problem is also analyzed in this section. Aiming at the practical problem analyzed in Section 2, a knowledge-based GSC method with an adaptive space filter is proposed in Section 3 and the availability is demonstrated in Section 4 with the measured data. Finally, conclusions are given in Section 5.

## 2. Generalized Side-Lobe Canceller

The GSC is proposed by Griffiths [11] and developed for adaptive noise cancellation by Jablon [10] and non-stationary hot-clutter cancellation by Abramovich [12]. It has been further analyzed and developed into the ionospheric clutter suppression in HFSWR for ocean remote sensing by Wan. In this section, we introduce the GSC method and a modified GSC method based on a virtual sliding subarray for greater system freedom.

### 2.1. Instruction of GSC

Assumption: the  $k$ -th sample of echo  $x(k)$  received by a  $N$ -element uniform linear array (ULA) is the sum of three components, as shown in Equation (1):  $s(k)$  indicates the SOI,  $c(k)$  indicates the interference and clutter, and  $n(k)$  indicates the noise:

$$\mathbf{x}(k) = \mathbf{s}(k) + \mathbf{c}(k) + \mathbf{n}(k) \quad (1)$$

In HFSWR, the noise can be treated as Gaussian distributed noise, which is uncorrelated, and the SOI can be expressed as  $\mathbf{s}(k) = \sqrt{N}A(k)\mathbf{a}_s$ , where  $\mathbf{a}_s$  is a vector which contains the direction of arrival (DOA) of the SOI,  $A(k)$  is the amplitude of the SOI and  $N$  is the number of elements.

The correlated matrix of the echo can be indicated as

$$\mathbf{R}_x = E[\mathbf{x}(k)\mathbf{x}^H(k)] = N\sigma_s^2\mathbf{a}_s\mathbf{a}_s^H + \mathbf{R}_{c+n} \quad (2)$$

where  $\sigma_s^2 = |A(k)|^2$  is the power of the signal and  $\mathbf{R}_{c+n}$  is the covariance matrix of the interference, clutter, and noise, which can be indicated as  $\mathbf{R}_{c+n} = E[\mathbf{c}(k)\mathbf{c}^H(k)] + \sigma^2\mathbf{I}$  where  $\sigma^2$  is the power of the noise.

According to the Minimum Variance Distortionless Response (MVDR) [21], the optimal adaptive beamforming vector  $\mathbf{w}$  corresponding to  $\mathbf{a}_s$  can be indicated as:

$$\mathbf{w} = \frac{\mathbf{R}_{c+n}^{-1}\mathbf{a}_s}{\mathbf{a}_s^H\mathbf{R}_{c+n}^{-1}\mathbf{a}_s} \quad (3)$$

In the practical radar system, the covariance matrix  $\mathbf{R}_{c+n}$  cannot be obtained in advance and it has to be estimated by secondary data. The GSC is an effective method utilizing the estimated covariance matrix to suppress the interferences and clutter. The framework of GSC is shown in Figure 1.

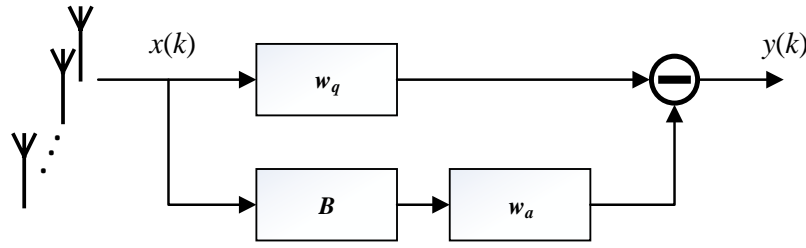


Figure 1. The framework of the GSC.

The echo obtained via the receiving array is weighted by the static weights  $w_q$ , which is the coefficients of digital beam forming (DBF) to keep the beam direction pointing at the SOI. The block matrix  $B$  is well-designed for obtaining the secondary data without the SOI.  $w_a$  is the adaptive weights vector, which is calculated by the estimation of the covariance matrix for interference and clutter suppression. Finally, the output of the GSC can be expressed as:

$$y(k) = (w_q - Bw_a)^H x(k) \quad (4)$$

$$w_q = \left( 1, e^{j\frac{2\pi}{\lambda}d \sin \theta}, e^{j\frac{2\pi}{\lambda} \cdot 2d \sin \theta}, e^{j\frac{2\pi}{\lambda}(N-1)d \sin \theta} \right)^H \quad (5)$$

where  $d$  is the interval of the adjacent elements,  $\lambda$  is the wavelength of working frequency and  $\theta$  is the expected beam pointing direction.

In this case, how to calculate the block matrix  $B$  and the adaptive weights  $w_a$  are the keys for the performance of the GSC. A proper block matrix  $B$  can keep the SOI out of secondary data which benefits the reduction of the SNR loss.

Let  $J = E[|y(k)|^2]$ , the constraint of MVDR [21] can be rewritten as an optimized problem:

$$\min_{w_a} J = \min_{w_a} (w_q - Bw_a)^H R_x (w_q - Bw_a) \quad (6)$$

where  $R_x = x(k)x^H(k)$  is the self-correlation matrix. For keeping the SNR loss minimized,  $R_x$  should only contain the interferences and clutter, excluding the SOI. Thus,  $R_x$  can be replaced by the covariance matrix of interference and clutter  $R_{c+n}$ , which contains all the clutter and interference in the side lobe. Then the optimized weights can be indicated as:

$$w_a = \left( B^H R_{c+n} B \right)^{-1} B^H R_{c+n} w_q \quad (7)$$

## 2.2. GSC Based on a Virtual Sliding Subarray

In Equation (7), the adaptive weights  $w_a$  for clutter suppression are obtained in the constraint of Equation (6) in which the covariance matrix  $R_{c+n}$  impacts the performance of suppression. For a better estimation of the covariance matrix  $R_{c+n}$ , the SOI must not be in the secondary data. Through dividing the whole receiving array into several subarrays and designing the block matrix  $B$ , the SOI can be rejected in the secondary data. Considering multi-target detection, a large degree of freedom of the system is necessary. Combining the above two considerations, a virtual sliding subarray (VSSA) is proposed. In this section, the GSC based on a virtual sliding subarray (VSSA-GSC) is introduced.

For an  $N$ -element uniform linear array, it is divided into  $N-N'+1$  sliding subarray which are formed by  $N'$  elements, as shown in Figure 2. The block matrix for the  $i$ -th sliding subarray  $B_i, i = 1, 2, \dots, N - N' + 1$  can be formed by a minimal  $P$ -norm single notch filter with the space response shown in Figure 3 where  $N = 32, N' = 12$ .

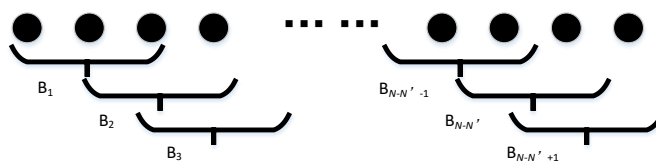


Figure 2. The framework of virtual sliding subarray.

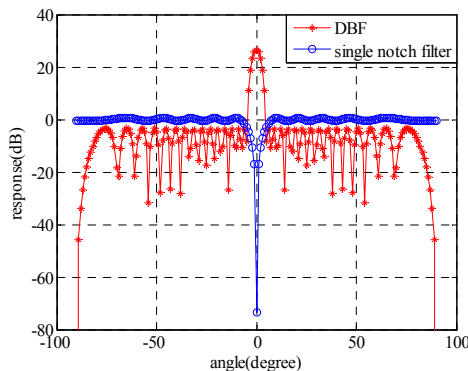


Figure 3. Space responses of DBF and a single notch filter with  $N = 32$  and  $N' = 12$ .

There are two beneficial features for obtaining secondary data by the minimal  $P$ -norm single notch filter:

- (a) The width of the notch is almost equal to the width of the main lobe: the SOI in the main lobe can be almost rejected and only the interferences and clutter are contained in the secondary data;
- (b) The side lobe of the filter is almost the same level with the side lobe: the interferences and clutter can be well expressed in the secondary data.

The VSSA-GSC can be completed via the following steps:

- (1). Design a minimal  $P$ -norm single notch filter with the coefficients  $c_j, j = 1, 2, \dots, N'$  to be the block matrix  $\mathbf{B}$ . The output of the  $i$ -th block matrix  $u_i$  is expressed as Equation (8) and the output of the  $i$ -th VSSA  $v_i$  is expressed as Equation (9). All the VSSA outputs form the data matrix  $\mathbf{U}$  and data vector  $\mathbf{V}$  as expressed in Equations (10) and (11);

$$u_i = \sum_{j=0}^{N'} c_j x_{i+j}(k), i = 1, 2, \dots, N - N' + 1 \tag{8}$$

$$v_i = \sum_{j=0}^{N'} w_{qj}^H x_{i+j}(k), i = 1, 2, \dots, N - N' + 1 \tag{9}$$

$$\mathbf{U} = \begin{bmatrix} u_1 & u_2 & \dots & u_{N-N'+1} \end{bmatrix}^T \tag{10}$$

$$\mathbf{V} = \begin{bmatrix} v_1 & v_2 & \dots & v_{N-N'+1} \end{bmatrix}^T \tag{11}$$

- (2). Calculate the self-correlation matrix  $\mathbf{R}_d$  and the cross-correlation matrix  $\mathbf{R}_0$  as Equations (12) and (13);

$$\mathbf{R}_d = \mathbf{U}\mathbf{U}^H \tag{12}$$

$$\mathbf{R}_0 = \mathbf{U}\mathbf{V} \tag{13}$$

(3). Calculate the adaptive weights  $w_a$  as Equation (14);

$$w_a = R_d^{-1} R_0 \tag{14}$$

(4). Finally obtain the output of VSSA-GSC by subtraction, as shown in Equation (15);

$$y(k) = (w_q - w_a)^H x(k) \tag{15}$$

The framework of VSSA-GSC is shown in Figure 4.

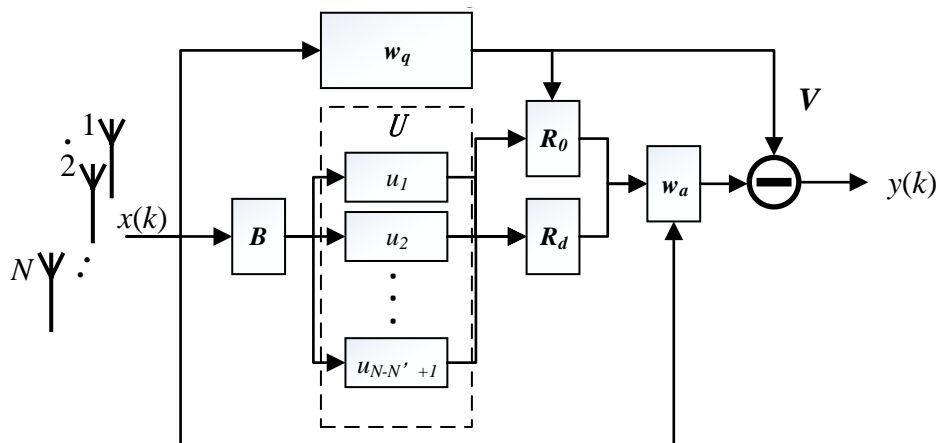


Figure 4. The framework of the VSSA-GSC.

### 2.3. Simulation of the VSSA-GSC

In this section, we try to verify the effectiveness of the VSSA-GSC via measured data obtained by a trail HFSWR system with a 32-element receiving array and with a simulation target injected into the measured data.

The range-Doppler frequency map with a beam direction of  $0^\circ$  of measured data is shown in Figure 5 with a working frequency  $f_0 = 5.2$  MHz, in which the beams are designed from  $-30^\circ$  to  $30^\circ$  with a  $3^\circ$  interval. The theoretic first-order Bragg frequencies are  $\pm 0.2326$  Hz according to the carrier frequency. Due to the current, the practical first-order Bragg frequencies are shifted. Ionospheric clutter appears around the 34th range bin in the direction of  $21^\circ$  as shown in Figure 5a,b.

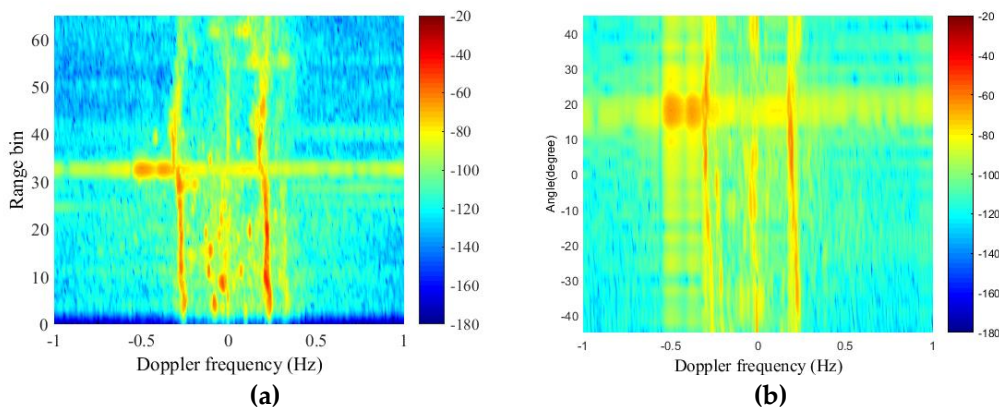


Figure 5. Range-Doppler frequency map: (a) range-Doppler map with the beam pointing to  $21^\circ$ ; (b) angle-Doppler map in the 34th range bin.

We consider two situations with the injected target to testify that the VSSA-GSC framework can make the SOI loss minimal and suppress the clutter at a maximum level:

**Situation a:** a visible target is injected into the non-clutter region to testify that the VSSA-GSC framework can make the SOI loss minimal;

**Situation b:** an invisible target is injected into the clutter region and it is submerged with the clutter to testify that the VSSA-GSC framework can suppress the clutter at a maximum level.

The details of the injected targets with constant speed are listed in Table 1.

**Table 1.** The information of the injected targets.

Situation	Range Bin	Doppler Frequency (Hz)	Angle (Degree)	SCR/SNR (dB)
<i>a</i>	42	−0.39	9	SNR = 35
<i>b</i>	34	−0.39	9	SCR = −5

In situation *a*, there is no ionospheric clutter in the area where the target is injected. In situation *b*, the target is injected into the Es-layer ionospheric clutter and the power is 5 dB stronger than the ionospheric clutter, but the SCR is not enough for detection. For signal processing, each VSSA is formed by 12 elements with the response shown in Figure 3 and 21 VSSAs are obtained. Following the algorithm described in Section 2.2, the targets in both situations are detected and the clutter in situation *b* is suppressed effectively, as shown in Figure 6a,b.

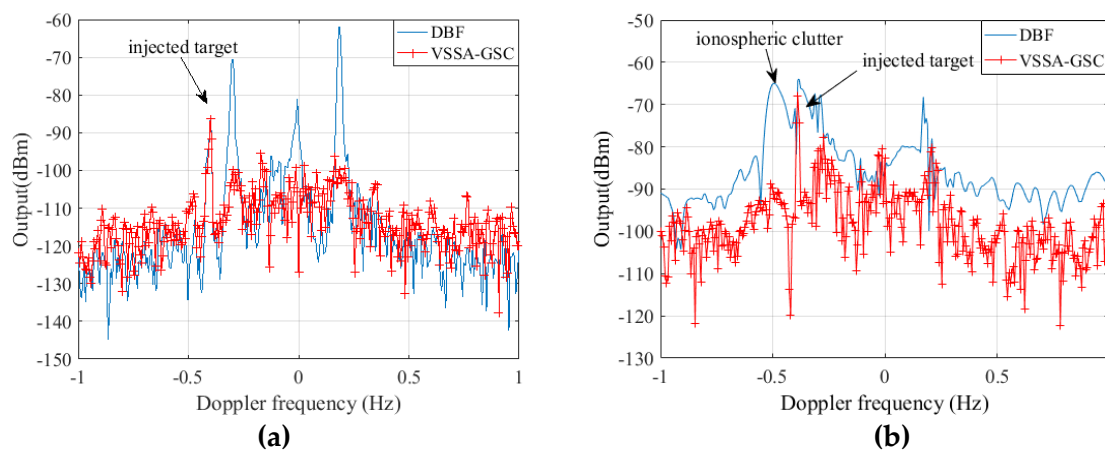


**Figure 6.** Doppler frequency profile: (a) visible target without clutter; (b) target submerged with clutter.

#### 2.4. Practical Problems

According to the previous simulation, VSSA-GSC is effective for suppressing the clutter in the side lobe. However, some practical factors must be considered carefully in the practical system, such as if the direction of the target is mismatched with the direction in which the beam is pointing.

Commonly, the beams of DBF point to several fixed directions which are designed elaborately due to the working frequency and the aperture of the receiving array. However, in the practical situation, targets emerging just at the direction the beam is pointing occurs with low probability. Under this consideration, the performance of VSSA-GSC is analyzed when a target emerging from between the adjacent beams in this section.

As shown in Figure 3, the depth of the notch is degraded seriously when the target is not at the direction in which the beam is pointing, which can lead to the SNR loss for strong targets in the trail HFSWR system as described above. An experiment is carried out in this section to analyse the relationship of SNR loss via the difference between the depth of the notch and input SNR when the input SNR is 30 dB. As shown in Figure 7, the SNR loss decreases as the difference decreases.

In order to guarantee the SNR loss less than 3 dB, the depth of the notch has to be 7 dB deeper than the input SNR.

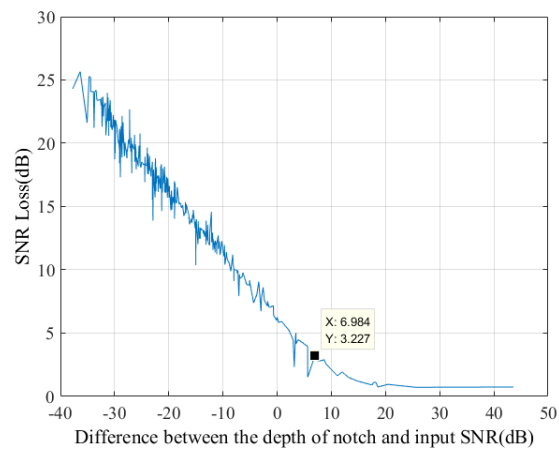


**Figure 7.** The relationship of SNR loss via difference between the depth of notch and inputted target SNR.

For the ideal situation, as simulated in Section 2.3, the injected targets in Table 1 are just emerging from the direction in which the beam is pointing. In this analysis, we adjust the direction of the target to make the target emerge from between the adjacent beams and the parameters of the target are the 34th range bin,  $f_d = -0.39$  Hz, a direction of  $20^\circ$  with an SNR = 15 dB. For further description, the beams of DBF near the injected target are  $18^\circ$  and  $21^\circ$  and the injected target is in a direction of  $20^\circ$  which is a  $1^\circ$  shift from the beam pointing at  $21^\circ$  and a  $2^\circ$  shift from the beam pointing at  $18^\circ$ . As shown in Figure 3, the depth of notch is  $-10.88$  dB when  $2^\circ$  is shifted from the beam pointing and  $-16.92$  dB when  $1^\circ$  is shifted from the beam pointing. With this block matrix  $B$ , the signal of target cannot be rejected thoroughly and it is contained in the secondary data obtained by the VSSA. In this case, the target in the main beam is cancelled by the output of the VSSA as shown in Figure 8.

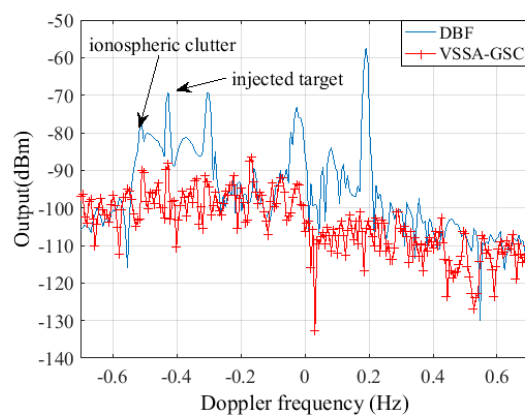


**Figure 8.** Doppler frequency profiles with DBF and VSSA-GSC.

To enhance the performance of VSSA-GSC, one key is optimizing the block matrix  $B$  to reject the signal of the target as thoroughly as possible.

### 3. Knowledge-Based VSSA-GSC

Aiming at the problem illuminated in Section 2.4, a knowledge-based VSSA-GSC (KB-VSSA-GSC) is developed for better detection of the target submerged in ionospheric clutter in this chapter.

The main idea of KB-VSSA-GSC is the single notch filter design adaptively based on two kinds of knowledge: system parameters and the energy of the strongest target detected without any clutter suppression.

The principle of adaptive single notch filter (ASNF) design follows two points:

**Point a:** the width of the notch should be wider than the width of the major beam according to the system parameters.

**Point b:** the depth of the notch should be deeper than the energy of the strongest target in the looking direction.

Therefore, the framework of the KB-VASS-GSC algorithm is shown in Figure 9. In this framework, a pre-detection module C and an ASNF design module A are added into the VSSA-GSC framework. In the next subsections the details of the innovative modules are introduced.

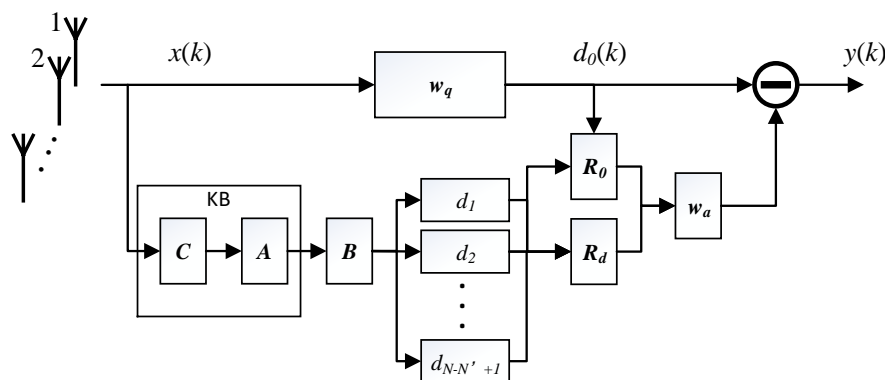


Figure 9. Framework of KB-VSSA-GSC.

### 3.1. Pre-Detection for Knowledge

The task of this module is to obtain the SNR of the strongest target detected without any clutter suppression. The maximum energy is treated as the knowledge for the ASNF design.

The Cell Averaging Constant False Alarm Rate (CA-CFAR) [22,23] method has been proved to be an effective method for pre-detection. The details of CA-CFAR are that of a classical algorithm and it is not the concern point of this paper. In this case, it is not described in this section.

Utilizing the CA-CFAR algorithm by setting a threshold which is 3.5 times that of the cell mean value, only the targets with high SNR can be detected. In this case, one of the factors for ASNF design which is the maximum SNR is obtained.

### 3.2. Adaptive Single Notch Filter Design

The most important key of KB-VSSA-GSC is how to design the ASNF. In this section, a novel adaptive notch filter is proposed based on spatial time symmetry and Fourier series expansion. Considering that HFSWR system operating at frequency  $f_0$  with an  $N$  element uniform linear array (ULA), the beamforming of the echo can be expressed as:

$$F(\theta) = \sum_{n=0}^{N-1} a_n(\theta_0) \cdot e^{-j \frac{2\pi}{\lambda/d} \sin \theta \cdot n} = \sum_{n=0}^{N-1} a_n(\theta_0) \cdot e^{-j \frac{2\pi}{\lambda/d} \sin \theta \cdot nd \cdot \frac{1}{d}} \quad (16)$$

where  $d$  is the distance between neighboring elements and  $\lambda$  is the wavelength.

Furthermore, the discrete Fourier series of the echo can be expressed as:

$$Y(k) = \sum_{n=1}^N y(n\Delta t) \cdot e^{-j \frac{2\pi}{M} \cdot kn\Delta t f_s} \quad (17)$$

where  $\Delta t$  is time sampling interval,  $f_s$  is sampling frequency, and  $M$  is the number of frequency components.

According to the definition of discrete Fourier series and the similarity between Equations (16) and (17), the relationship between space frequency and angle is given by Equation (18):

$$f' = \frac{\sin \theta}{\lambda/d} \cdot \frac{1}{d} = \frac{\sin \theta}{\lambda} = \frac{f_0 \cdot \sin \theta}{c} \quad (18)$$

Based on exponential formula, the main-lobe width is expressed as:

$$\theta_m = 51.05 \cdot \frac{c}{(N-1) \cdot d \cdot f_0} \quad (19)$$

Inserting Equation (19) into (18), the space frequency is obtained by:

$$f'_m = \frac{f_0 \cdot \sin \left( 51.05 \cdot \frac{c}{(N-1) \cdot d \cdot f_0} \right)}{c} \quad (20)$$

According to Equation (20) and Fourier series expansion, the spatial response function of the proposed ANSF is expressed as Equation (21):

$$H(e^{j\omega'}) = \begin{cases} e^{-j\omega'a} & \omega'_c \leq |\omega'| < \pi \\ 0 & 0 \leq |\omega'| < \omega'_c \end{cases} \quad (21)$$

where  $\omega' = 2\pi f'$  is the space frequency,  $\omega'_c$  is the cut-off frequency.  $\omega'_p$  is the spatial pass-band cut-off frequency,  $\omega'_s$  is the spatial stop-band cut-off frequency. In an ideal situation  $\omega'_c = \omega'_s = \omega'_p$ , the notch filter would acquire optimal performance. However, under the real situation, we can only get  $\omega'_p$  which is close to  $\omega'_s$  owing to the limit of the array aperture; Right now, we expect  $\omega'_c = (\omega'_s + \omega'_p)/2$ . Aiming to ensure that the pass-band of the space notch filter is no less than the main-lobe width,  $\omega'_s$  should meet  $\omega'_s = 2\pi f'_m$ .

The unit impulse response [24] of the proposed spatial notch filter is expressed as shown in Equation (22)

$$h(n') = \begin{cases} \frac{\sin[\pi(n' - a)]}{\pi(n' - a)} - \frac{\sin[\omega'_c(n' - a)]}{\pi(n' - a)} & n' \neq a \\ 1 - \frac{\omega'_c}{\pi} & n' = a \end{cases} \quad (22)$$

where  $a = (N' - 1)/2$ , and  $N'$  is the order of the filter.

Implementing the spatial notch filter needs the number of the antenna elements. The coefficients of the filter portray an even symmetry, so that,  $N'$  is the odd number and can be given by Equation (23), owing to the empirical formula [24]:

$$N' = \left\lceil \frac{A - 8}{2.285 |\omega'_p - \omega'_s|} \right\rceil \quad (23)$$

where  $\lceil x \rceil$  is the ceiling of  $x$ , and  $A$  and  $\omega'_s$  must be no less than the maximum SNR detected by the CA-CFAR in the pre-detection of the monitoring region and main-lobe width separately, which ensures avoiding the problem revealed in Section 2.4, while  $\omega'_p$  needs to be adjusted according to the practical elements appropriately. In the practical system, the Fourier series is truncated by the limited elements

$N'$ , which brings about the Gibbs phenomenon, and then extremely degrades the performance of the filter. For the reason, a Kaiser window which is expressed as Equation (24) is employed.

$$w(n') = \frac{I_0(\beta\sqrt{1 - [1 - 2n'/(N' - 1)]^2})}{I_0(\beta)}, 0 \leq n' \leq N' - 1 \quad (24)$$

where  $I_0(\cdot)$  is the First Class Zero-order Modified Bessel Function,  $\beta$  is a variable parameter for the selecting the main beam width and side lobe attenuation. Consequently, the modified unit impulse response of the spatial notch filter is developed as Equation (25)

$$h_d(n') = h(n') * w(n') \quad (25)$$

The order of ANSF  $N'$ , which is also the number of elements in VSSA, is calculated by Equation (23) which depends on the maximum SNR  $A$  and the width of main-lobe  $\omega'_s$ . In theory, the length  $N'$  can affect the maximum number of detecting targets and the maximum number of interferences suppressed. This means that  $N'$  should be larger if more targets need to be detected and  $N'$  should be smaller if more interferences need to be suppressed. In this case, the length  $N'$  should be designed based on the system requirements.

According to the measured data parameters used in Section 2, and considering that the maximum SNR of the suspected targets in the main lobe is 35 dB, which is the output of the pre-detection module, the space responses of the proposed ASNF is shown in Figure 10, where the filter order is  $N' = 12$  and the expected angle attenuation is  $-47.22$  dB. The compared space response results of the ASNF and single notch filters chosen in Figure 3 are shown in Figure 10. It can be seen from Figure 10 that ASNF is much better than the single notch filter for absolutely rejecting main-lobe information and retaining the side-lobe information as much as possible.

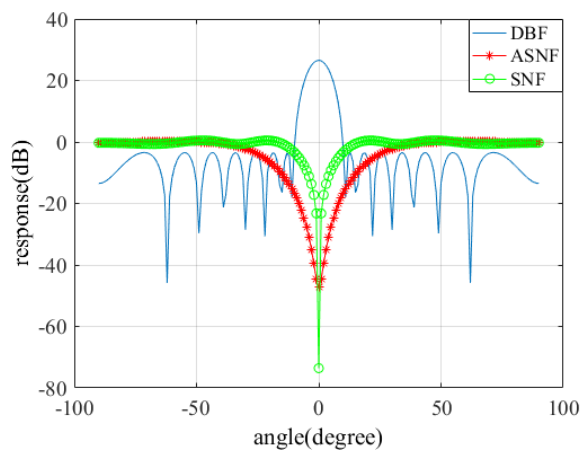


Figure 10. Space responses of DBF and two single notch filters.

#### 4. Results of the Measured Data

The experiments are carried out in this section to verify the preceding framework using measured data as shown in Figure 8 (Section 2.3). For one simulated target at beam direction  $\varphi = 20^\circ$ ,  $f_d = -0.3878$  Hz, and the 34th range bin are injected into the measured data. The adjoining beams of the system are  $18^\circ$  and  $21^\circ$ . Utilizing VSSA-GSC without ANSF, the injected target is cancelled as the ionospheric clutter is cancelled. Opposite, KB-VSSA-GSC with a 12-order ASNF can make the injected target visible as the ionospheric clutter is suppressed and the SCR is improved 14 dB, respectively, as shown in Figure 11.

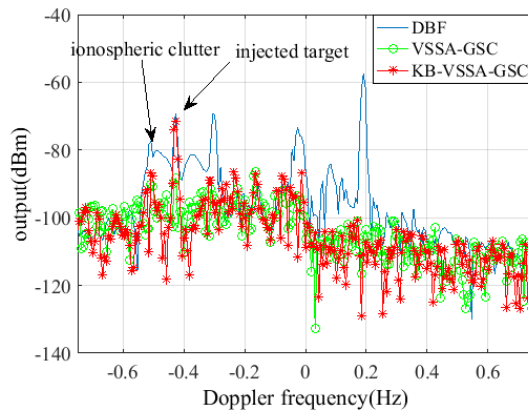


Figure 11. Doppler frequency profile with KB-VSSA-GSC.

To underline the advantage gained, Figures 12 and 13 plot: when the target is shifted 1° from the main beam, the changing curves of single notch filter output SNR ( $SNR_F$ ), and the GSC output SNR ( $SNR_{OUT}$ ) according to the input SNR (Figure 12) and the changing curves of SNR loss according to the input SNR (Figure 13) both for 10,000 Monte Carlo experiments.

The relation between  $SNR_F$ ,  $SNR_{OUT}$ , input SNR and SNR Loss are:

$$SNR_{OUT} = \text{input SNR} - SNR_F \tag{26}$$

$$SNR \text{ Loss} = \text{input SNR} - SNR_{OUT} \tag{27}$$

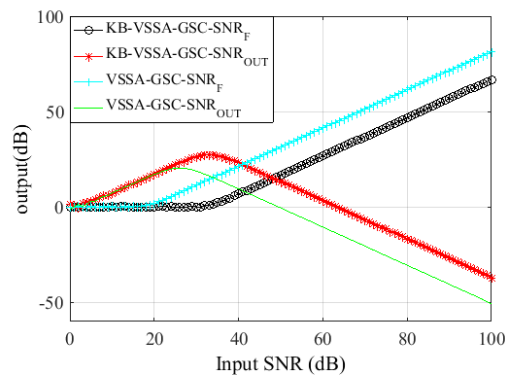


Figure 12. Single notch filter output SNR ( $SNR_F$ ) and GSC output SNR ( $SNR_{OUT}$ ).

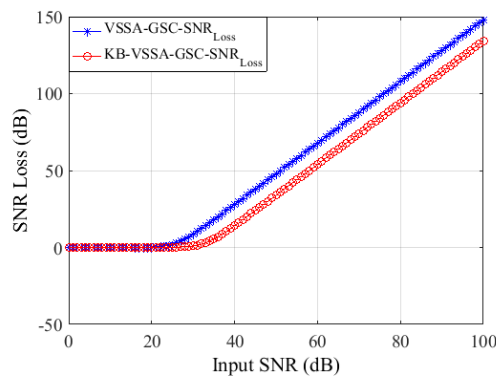


Figure 13. SNR loss of VSSA-GSC and KB-VSSA-GSC.

For VSSA-GSC, as the input SNR increases to 20 dB,  $SNR_{OUT}$  decreases due to that the single notch filter cannot reject the target clearly. SNR loss increases. As the input SNR increases to 50 dB,  $SNR_{OUT}$  is negative which means the noise is amplified. Opposite, KB-VSSA-GSC can cause no SNR loss if the input SNR is less than 35 dB, which is just equal to the maximum SNR obtained by the pre-detection module. Furthermore, the noise may be amplified when the input SNR equals to 61 dB, which cannot happen as the maximum SNR is 35 dB.

According to the comparisons above, it is clear that the KB-VSSA-GSC algorithm we proposed still works well in the practical situations.

## 5. Conclusions

In this paper, we propose a novel knowledge-based virtual sliding subarray generalized side lobe canceller (KB-VSSA-GSC) structure for the situation where a target emerges from between the adjacent beams as the performance of the GSC algorithm degrades significantly. The benefits are obtained by a well-designed adaptive spatial notch filter according to the width of main beam and maximal suspected target energy in the respective beams. The KB-VSSA-GSC algorithm is validated by measured data which shows that clutter suppression performance can be notably improved in the background of a target emerging between the adjacent beams. How to design a better performing filter in the limited elements situation will be further discussed in future research.

**Acknowledgments:** The authors are grateful to the Institute of Electronic and Information Technology, who provided the HFSWR data and those who helped during the writing of this paper. This work is supported by the National Natural Science Foundations of China (61701140), Project funded by Heilongjiang Postdoctoral Science Foundation (LBH-Z17093) and the Fundamental Research Funds for the Central Universities (Grant No. HIT.NSRIF.2018/5).

**Author Contributions:** Xin Zhang as the main author proposed the method, designed and conducted the experiments, performed the data processing and analysis, and wrote the manuscript. Di Yao, Qiang Yang, and Yingning Dong reviewed the manuscript and contributed to discussions. Weibo Deng supervised and advised the research work.

**Conflicts of Interest:** The authors declare no conflict of interest.

## References

1. Barton, D.K.; Leonov, S.A. *Radar Technology Encyclopedia*, 3rd ed.; Artech House: Norwood, MA, USA, 1998; pp. 201–203, ISBN 0-89006-893-3.
2. Mao, T.; Xia, W.; Qu, C.P.; Luo, J. A study on characteristics and applications of HF ground wave OTH radar. *Mod. Radar* **2009**, *31*, 7–10.
3. Ravan, M.; Adve, R.S. Ionospheric Clutter Model for High Frequency Surface Wave Radar. In Proceedings of the 2012 IEEE Radar Conference, Atlanta, GA, USA, 7–11 May 2012. [[CrossRef](#)]
4. Jiang, W.; Deng, W.B. Characteristic research of ionospheric clutter in over the horizon HFSWR. In Proceedings of the 2009 IET International Radar Conference, Guilin, China, 20–22 April 2009; pp. 1–8. [[CrossRef](#)]
5. Zhao, L.; Society, I.C. A model for the Ionospheric Clutter in HFSWR Radar. In Proceedings of the International Conference on Information Management, Innovation Management and Industrial Engineering, Taipei, Taiwan, 19–21 December 2008; pp. 179–182. [[CrossRef](#)]
6. Peter, M.; Tony, P.; David, D.; Rick, M.; Nathan, K.; Yannick, A. Canada's Radar System Third Generation High Frequency Surface Wave. *J. Ocean. Technol.* **2015**, *10*, 2.
7. Anthony, P.; Rick, M.R.; Zhen, D.; Peter, M.; Derek, Y. Towards a Cognitive Radar: Canada's Third-Generation High Frequency Surface Wave Radar (HFSWR) for Surveillance of the 200 Nautical Mile Exclusive Economic Zone. *Sensors* **2017**, *17*, 1588. [[CrossRef](#)]
8. Ponsford, A.M. Raytheon Company, Persistent Surveillance of the 200 nautical mile, Exclusive Economic Zone (EEZ) using land-based High Frequency radar. *Can. J. Remote Sens.* **2001**, *27*, 354–360. [[CrossRef](#)]
9. Sevgi, L.; Ponsford, A.; Chan, A. An integrated maritime surveillance system based on high frequency surface wave radars, Part 1—Theory of operation. *IEEE Proc. Antennas Propag.* **2001**, *43*, 28–43. [[CrossRef](#)]

10. Sevgi, L.; Ponsford, A.; Chan, A. An integrated maritime surveillance system based on high frequency surface wave radars, Part 2: Operational status and system performance. *IEEE Proc. Ant. Prop.* **2001**, *43*, 52–63. [[CrossRef](#)]
11. Buckley, M.K.; Griffiths, L.J. An adaptive generalized sidelobe canceller with derivative constraints. *IEEE Trans. Antennas Propag.* **1986**, *34*, 311–319. [[CrossRef](#)]
12. Abramovich, Y.I.; Spencer, N.K.; Anderson, S.J.; Gorokhov, A.Y. Stochastic-constraints method in nonstationary hot-clutter cancellation. I. Fundamentals and supervised training applications. *IEEE Trans. Aerosp. Electron. Syst.* **1998**, *34*, 1271–1292. [[CrossRef](#)]
13. Abramovich, Y.I.; Spencer, N.K.; Anderson, S.J. Stochastic-constraints method in nonstationary hot-clutter cancellation. II. Unsupervised training applications. *IEEE Trans. Aerosp. Electron. Syst.* **2000**, *36*, 132–150. [[CrossRef](#)]
14. Fabrizio, G.A.; Gershman, A.B.; Turley, M.D. Robust adaptive beamforming for HF surface wave over-the-horizon radar. *IEEE Trans. Aerosp. Electron. Syst.* **2004**, *40*, 510–525. [[CrossRef](#)]
15. Jablon, N. Adaptive beamforming with the generalized sidelobe canceller in the presence of array imperfections. *IEEE Trans. Antennas Propag.* **1986**, *34*, 996–1012. [[CrossRef](#)]
16. Haohai, S.; Shefeng, Y.; Svensson, U.P. Robust spherical microphone array beamforming with multi-beam-multi-null steering, and sidelobe control. In Proceedings of the WASPAA '09. IEEE Workshop on Applications of Signal Processing to Audio and Acoustics, 2009, New Paltz, NY, USA, 18–21 October 2009; pp. 113–116. [[CrossRef](#)]
17. Karakutuk, S.; Agirman, H. Adaptive interference cancellation using microphone arrays. In Proceedings of the 2014 22nd Signal Processing and Communications Applications Conference (SIU), Trabzon, Turkey, 23–25 April 2014; pp. 1766–1769. [[CrossRef](#)]
18. Wan, X.; Cheng, F.; Ke, H. Sporadic-E ionospheric clutter suppression in HF surface-wave radar. In Proceedings of the 2005 IEEE International Radar Conference, Arlington, VA, USA, 9–12 May 2005; pp. 742–746. [[CrossRef](#)]
19. Wan, X.R.; Ke, H.Y. Adaptive ionospheric clutter suppression based on subarrays in monostatic HF surface wave radar. *IEE Proc. Radar Sonar Navig.* **2005**, *152*, 89–96. [[CrossRef](#)]
20. Thayaparan, T.; MacDougall, J. Evaluation of ionospheric sporadic-E clutter in an Arctic environment for the assessment of High-Frequency Surface-Wave Radar surveillance. *IEEE Trans. Geosci. Remote Sens.* **2005**, *43*, 1180–1188. [[CrossRef](#)]
21. Van Trees, H.L. *Optimum Array Processing—Part IV of Detection, Estimation and Modulation Theory*; John Wiley & Sons: New York, NY, USA, 2002; ISBN 9780471093909.
22. Gandhi, P.P.; Kassam, S.A. Analysis of CFAR processors in nonhomogeneous background. *IEEE Trans. Aerosp. Electron. Syst.* **1988**, *24*, 427–445. [[CrossRef](#)]
23. Fernandez, J.R.M.; Martinez, S.T.; Vidal, J.D.B. CA-CFAR Adjustment Factor Correction with a priori Knowledge of the Clutter Distribution Shape Parameter. *Int. J. Interact. Multimed. Artif. Intell.* **2017**, *4*, 7–13. [[CrossRef](#)]
24. Oppenheim, A.V.; Schaffer, R.W. *Discrete-Time Signal Processing*, 3rd ed.; Prentice Hall: Boston, MA, USA, 2009; pp. 540–574, ISBN 9780131988422.



© 2018 by the authors. Licensee MDPI, Basel, Switzerland. This article is an open access article distributed under the terms and conditions of the Creative Commons Attribution (CC BY) license (<http://creativecommons.org/licenses/by/4.0/>).